Causal Discovery and Injection for Feed-Forward Neural Networks

Fabrizio Russo[1] **and Francesca Toni**[1]
[1] Imperial College London
fabrizio@imperial.ac.uk, ft@imperial.ac.uk

Abstract

Neural networks have proven to be effective at solving a wide range of problems but it is often unclear whether they learn any meaningful causal relationship: this poses a problem for the robustness of neural network models and their use for high-stakes decisions. We propose a novel method overcoming this issue by injecting knowledge in the form of (possibly partial) causal graphs into feed-forward neural networks, so that the learnt model is guaranteed to conform to the graph, hence adhering to expert knowledge. This knowledge may be given up-front or during the learning process, to improve the model through human-AI collaboration. We apply our method to synthetic and real (tabular) data showing that it is robust against noise and can improve causal discovery and prediction performance in low data regimes.

1 Introduction

Causal knowledge is key in establishing robust relationships between causes and effects towards creating scientific knowledge. The causal mechanisms that drive behaviours observed in nature are stable and described by Pearl [2009] as *deterministic functional relationships* organised in an acyclic structure. Causal discovery and causal Bayesian networks have been used to study these mechanisms for a while [Pearl and Verma, 1991, Heckerman et al., 1995] with the idea that external causal knowledge can be integrated with observational data and obviate to the limitations thereof (e.g. noise and spurious correlations).

Neural networks have proven to be very effective at solving a wide range of problems [Goodfellow et al., 2016] but it is often unclear whether they learn any meaningful causal relationship, as proven by their weakness to data perturbation and adversarial attacks [Szegedy et al., 2013, Goodfellow et al., 2014]. This inability of neural networks to truly *understand* the data and their tendency to establish spurious relationships poses a problem for the robustness of this type of model and their use for high-stakes decisions [Rudin, 2019].

To address this problem, taking into account causal relationships during training (e.g. as in [Zhang et al., 2020, Kyono et al., 2020, Li et al., 2021]) has been shown to result in more reliable neural networks, focusing on stable relationships rather than spurious ones. In this paper we contribute to this line of work by making neural networks adhere to expert knowledge representing causal relationships for all available (input and output) features or a subset thereof, so that the causality structure that is believed to govern the problem analysed (and the data representing it) is respected by the learnt models. This allows the learning to focus on stable relationships [Pearl, 2009] only, without the "distraction" of spurious relationships deriving from noisy data.

Bridging the gap between causality and neural networks not only serves the purpose of making them more robust and reliable, but also has the potential of making them more *interpretable*. A few works have recently attempted to interpret neural networks as causal structures [Alvarez-Melis and Jaakkola, 2017, Chattopadhyay et al., 2019, Schwab and Karlen, 2019], but these represent the causal relationships within the models. Instead, our aim in this paper is to enforce a causal structure drawn from the real world onto neural networks. Specifically, we make the following contributions:

- We propose an algorithm to *inject*, into feed-forward neural networks, causal knowledge in the form of directed acyclic graphs (DAGs), so that the learnt model is guaranteed to use only the relationships specified therein, hence adhering to expert knowledge captured by the DAG.
- We propose a second algorithm for *human-AI collaboration* on the causal discovery task, to be (possibly) carried out prior to the causal injection of the first algorithm ; this algorithm takes, in input, graphs representing partial causal relationships as well as feedback from humans on computed DAGs, to obtain a feed-forward neural network model conforming to the input graphs and the human feedback.
- We apply our algorithms to (synthetic and real) tabular data showing that: (i) causal DAGs can be learned, with our method, from a relatively small amount of data; (ii) injecting partial knowledge improves causal discovery in low data regimes; (iii) our methods can improve feed-forward neural networks' predictive performance while making the models significantly more parsimonious, in line with the DAG they compute and adhere to; (vi) in the event that the predictive performance is

negatively impacted by the causal assumptions injected, the worsening is generally insignificant, while the gain in parsimony and interpretability is conspicuous.

The paper is organised as follows: we start with related work (Section 2), followed by the necessary notation and techniques we build upon (Section 3). We then introduce our novel algorithms (Section 4), for dealing with complete and partial causal knowledge , and demonstrate empirically their performance and utility (Section 5). We conclude, discussing directions for future work (Section 6).

2 Related Work

Causality underpins the creation of human knowledge, regulates physical reality as well as human understanding thereof. The mathematisation of causality has allowed scientists to solve paradoxes and answer questions regarding cause-effect relationships in many fields from biological to social sciences [Pearl, 2009]. The causal discovery framework proposed by Pearl [2009] includes two main concepts: *causal structure* in the form of a DAG, and a *causal model* that extends this structure by describing the functional relationships represented by the edges of the graph. In this paper we adopt the former, and focus on addressing the limited availability of such DAGs for applications , by allowing human-AI collaboration for knowledge discovery to be guided by partial knowledge injection . In fact, the automation of the causal discovery task and its wherewithal have been long discussed [Pearl, 2009].

(Bayesian) Causal networks [Pearl, 2009], together with algorithms to learn their structure (e.g. as in Pearl and Verma [1991], Spirtes et al. [1993], Heckerman [2013]), are the go-to when predicting cause-effect relationships. The recent rebound of deep learning and the ability of large neural networks to solve difficult problems in fields like computer vision and natural language processing (NLP) [Goodfellow et al., 2016] raise a question around causality: can we leverage the power of neural models but "discipline" them by enforcing a human-driven causal view of the world? The two disciplines have come closer only in recent years Schölkopf [2019] with benefits from both sides.

In this paper, we contribute to causal discovery with neural networks. For recent overviews of causal discovery methods we refer the reader to Glymour et al. [2019], Guo et al. [2020], Vowels et al. [2021]. In general, it is known that causal discovery with observational data is an NP-hard problem involving non-convex optimisation. Some Pearl and Verma [1991], Spirtes et al. [1993], Heckerman [2013] have adopted a Bayesian statistical methodology involving expert knowledge to drive the learning. Recent advances have translated the underlying combinatorial optimisation problem into a continuous (hence more tractable) version [Lachapelle et al., 2020, Zheng et al., 2018, 2020]. Causal discovery has been proposed also through the use of time series data with Convolutional Neural Networks [Nauta et al., 2019] or conditional transfer entropy [Aste and Di Matteo, 2017]. Other techniques applied to the problem include meta-learning [Bengio et al., 2019], reinforcement learning [Zhu et al., 2020] or generative networks [Goudet et al., 2017] that simulate the world and its different states to then evaluate the possible causal relationships governing it.

Specifically, in this work we leverage on a recent methodology employing causal discovery to improve neural models, i.e. Causal Structure Learning (CASTLE) [Kyono et al., 2020]. This approach exploits the causal DAG discovery methods in [Zheng et al., 2018, 2020] to shrink the weights of the non-causal predictors and regularize the neural network to make it more robust to noise and data shifts, through causality. Our algorithms build upon CASTLE, but *inject* expert knowledge while conducting causal discovery, forcing the neural networks to abide by the "guidance" provided by the experts.

Our approach injects causal knowledge in the form of DAGs and/or graphs. Thus, it differs from recent work in injection of causal knowledge into neural architectures in the NLP domain [Li et al., 2021], which uses instead labelled examples (pairs of words or sentences) to perform causal injection for natural language causal inference tasks, by tuning a pre-trained language models such as BERT.

Other frameworks integrating structural causal models and deep learning components include the recent works by [Pawlowski et al., 2020] and [Xia et al., 2021]. Both these works focus on causal inference rather than discovery. In the former, the edges in an input causal graph are modelled through normalising flows using neural components to estimate some of the necessary parameters. In the latter, a novel objective function is proposed to compute the identifiability of the causal effects (given a DAG) estimated through a masked autoencoder Germain et al. [2015]. Like [Pawlowski et al., 2020], and unlike [Xia et al., 2021], we analyse the simpler case where there are no unobserved confounders. Unlike both of them, for the purposes of this paper, we are not concerned with causal estimation and inference but only with discovery, aiming at investigating how injecting partial causal knowledge can improve both discovery and interpretability, without hurting (and possibly even improving) predictive performance. Given that we are not dealing with causal inference, when we talk about predictive performance, means that we are still on the first rung of Pearl's causality ladder Pearl [2009]. We leave to future work the exploration of causal inference within (suitable extensions of) our methods.

3 Preliminaries

In this section we introduce notation , basic notions in causality, and finally provide a technical overview of the essential components of CASTLE, which we use as a starting point for causal discovery.

Set-up. Let $X_1, \ldots, X_d$ be the set of *input features* and Y be the *target feature* within a regression or classification setting, with X_k (for $k \in \{1, \ldots, d\}$) taking values in $\mathcal{X}_k$ (e.g. $\mathcal{X}_k = \mathbb{R}$) and Y taking values in $\mathcal{Y}$ (e.g. $\mathcal{Y} = \mathbb{R}$) . Let $\mathcal{X} = \mathcal{X}_1 \times \ldots \times \mathcal{X}_d$. We denote with $f_Y : \mathcal{X} \to \mathcal{Y}$ a function that maps assignments of values $[x_1, \ldots, x_d] \in \mathcal{X}$ to the input features onto a value $y \in \mathcal{Y}$ for the target feature Y.[1] In practice, f_Y is learnt from a training dataset $\mathcal{D} = \{(x_i, y_i) | i \in \{1, \ldots, N\}, x_i \in \mathcal{X}, y_i \in \mathcal{Y}\}$ (assumed to be drawn from a joint distribution of values for input and target features).

[1] As in Pearl [2009], we use lower-case to represent values assigned to features, in upper-case.

Causal structures and models. As in Pearl [2009] , we use directed acyclic graphs (DAGs) to represent *causal structures* over input and target features, where a DAG $\mathcal{G}$ is a pair $\langle V, E \rangle$ with $V = \{X_1, \ldots, X_d, Y\}$ the set of vertices and $E \subseteq V \times V$ the set of edges of $\mathcal{G}$. A *causal model* is given by a DAG with accompanying structural equations of the form $v_i = f_i(pa_i, u_i)$ where v_i is a value for $i \in V$ with parents Pa_i having values pa_i, for f_i a function and u_i representing the errors due to omitted features.

CASTLE This approach operates with a feed-forward neural network combining $d+1$ sub-networks, each with d input neurons, amounting to all input and target features minus one (i.e. each sub-network "masks" a distinct element amongst $X_1, \ldots, X_d, Y$). All sub-networks have $M+1$ layers, and differ only in the input and output layers (i.e. layers $2, \ldots, M$ are shared). The output layer of a sub-network with feature F "masked" in the input layer amounts to output neuron F. Thus, each sub-network is responsible for reconstructing one feature. Overall, the network has an input layer with $(d+1) \cdot d$ neurons and an output layer with $d+1$ neurons. We will refer to the feed-forward neural network, with all its sub-networks, as the *joint network*. We will also refer to weights for layer $l \in \{1, \ldots, M\}$ as Θ_l, where $\Theta_l^{i,j}$ is the weight from neuron i in layer l to neuron j (in layer $l+1$) and, moreover, $\Theta_1^{i,j,k}$ stands for the weight from input neuron i in layer 1 to neuron j (in the first hidden layer) within the k-th sub-network. A schematic view of the joint network can be found in Appendix A, Figure 4.

The joint network is used for both prediction (for the target feature) and reconstruction (of the input features, where the k-th sub-network aims at reconstructing the k-th feature amongst $X_1, \ldots, X_d, Y$, thus acting as a sort of autoencoder). Furthermore, the joint network is used to obtain an adjacency matrix $\mathbf{W} = (w_{ik})$ for any $i, k \in \{1, \ldots, d+1\}$ whose elements w_{ik} result from the square root of the sum of squared input layer weights across the hidden neurons. Formally, for h the number of hidden neurons in the first hidden layer:[2]

$$w_{ik} = \sqrt{\sum_{j=1}^{h} \left(\Theta_1^{i,j,k}\right)^2} \tag{1}$$

Thus, $\mathbf{W}$ is a square hollow matrix of order $(d+1)$ holding a non-negative weight for each feature (including the target) from and towards all the others.

Like CASTLE, we use classic back-propagation and gradient descent optimisation applied to the "augmented" loss function from 'NOTEARS' [Zheng et al., 2018, 2020]. The overall loss is formed by two components: the prediction loss and the *DAG loss*. The former is the usual Mean Squared Error (MSE) or cross-entropy loss (for regression and classification respectively). The DAG loss is from Zheng et al. [2018] and can itself be decomposed into three components: the reconstruction loss (MSE for each of the inputs, assuming they are continuous), the acyclicity loss (a term that is 0 when $\mathbf{W}$ represents a DAG, from Theorem 1 of Zheng et al. [2018]) and a L_1 loss to induce further sparsity in the weights' matrix.

[2] We assume that $\Theta_1^{i,j} = 0$ for i the "masked" neurons.

The interested reader can find details on the definition of the (background) notion of loss in Zheng et al. [2018], Kyono et al. [2020].

4 Methodology

Our objective is to inject causal knowledge into neural networks, so that a user can have the confidence that their model is establishing and leveraging causal (i.e. robust, intuitive and general) relationships in its predictions (or more in general in its analysis of the data). In this section we first introduce the algorithm we devised to inject (discovered or pre-existing) causal knowledge, in the form of a *full* DAG (i.e. a DAG deemed to capture all applicable causal relationships amongst features) into a feed-forward neural network (Section 4.1). In practice, though, having a full DAG is rare. Thus, we propose an additional algorithm that takes in input a *graph imposing hard constraints* on relationships between features and (i) injects the graph into the model while discovering causal relations as well as (ii) allowing for the refinement of the resulting full DAG through human experts' input to then make the model adhere to it.

4.1 The Causal Graph Injection Algorithm

Our algorithm for causal injection into feed-forward neural networks takes three main inputs: a training dataset $\mathcal{D}$, a joint network randomly initialised or, better, already fitted on $\mathcal{D}$, with resulting weights Θ_t and a causal DAG $\mathcal{G}$. The output amounts to a *masked* joint network with weights Θ_T, which only uses the relationships contemplated in $\mathcal{G}$, and an adjacency matrix of the form of Equation 1 , which can be transformed into $\mathcal{G}$ (using Equation 2 given later).

The general method to induce a neural network to adhere to an input DAG is provided in Algorithm 1. The algorithm aims at fitting the joint neural network, possibly tuning a pretrained joint network, forcing it to use only the relationships (the edges $(i, j) \in E$ of the input DAG $\mathcal{G}$) that have been accepted by the modeller (and thus are part of $\mathcal{G}$). The injection is achieved through masking the weights of the input layer not having a counterpart in the input graph (i.e the missing edges).

The loss is as proposed by Zheng et al. [2018], Kyono et al. [2020] (see Section 3; in Algorithm 1 we use $\mathcal{L}_t$ to indicate the loss at iteration t), and computed by the `update()` function after backpropagation, but the algorithm focuses the training on the weights for the accepted edges, i.e. the causal relationships. The `update()` function will refine the network's weights to be effective in the prediction and reconstruction tasks without the aid of the spurious non-causal relationships. $\mathbf{W}_\mathcal{G}$ is a simple transformation of the learnt weights Θ_T after convergence: the latter will result from progressive changes , for a number of steps that is at most T but could be less if the *patience* threshold $T_s < T$ is reached (namely if no reduction of the loss function is achieved for T_s consecutive steps) .

The original CASTLE regularises the underlying neural network through an objective function that "shrinks" weights so that the fitted model uses, for the predictions, parents *more than* children and siblings (as represented by the adjacency matrix resulting from Equation 1). In contrast, our Algorithm 1 *enforces* the use of parents, instead of only preferring

Algorithm 1 Inject Causal DAG

Input: Training Data $\mathcal{D}$; network with M layers, h neurons in the first hidden layer, trained for t steps with final weights Θ_t ; max number of steps T; patience $T_s < T$; causal DAG $\mathcal{G} = \langle V, E \rangle$

Function: `DAG_inject`$(\mathcal{D}, \Theta_t, T, T_s, \mathcal{G})$:

for $i, k \in \{1, \dots d+1\}$ **do**
  for $j \in \{1, \dots, h\}$ **do**
    if $(i,k) \notin E$ **then**
      $\Theta^{i,j,k}_{1,t+1} \leftarrow 0$ ▷ mask non-causal relations
    else
      $\mathcal{L}_{\text{best}}, t_s \leftarrow 1e9, 0$
      while $t < T$ & $t_s < T_s$ **do**
        $\Theta^{i,j,k}_{1,t+1} \leftarrow$ `update`$(\Theta^{i,j,k}_{1,t}, \mathcal{D})$ ▷ causal relations
        $\Theta_{m,t+1} \leftarrow$ `update`$(\Theta_{m,t}, \mathcal{D})$ $\forall m \in \{1, \dots, M\}$
        $t \leftarrow t + 1$
        if $\mathcal{L}_t < \mathcal{L}_{\text{best}}$ **then**
          $\mathcal{L}_{\text{best}}, t_s \leftarrow \mathcal{L}_t, 0$
        else
          $t_s \leftarrow t_s + 1$
        end if
      end while
    end if
  end for
end for
$\Theta_T \leftarrow \Theta_t$
$\mathbf{W}_{\mathcal{G}} \leftarrow$ `apply`(Eq.1, Θ_T)
return $\mathbf{W}_{\mathcal{G}}, \Theta_T$

Output: Adjacency matrix $\mathbf{W}_{\mathcal{G}}$, Revised weights Θ_T

it: we reconstruct each feature and carry out the target prediction using *only* the feature's parents (this is implicit in Algorithm 1, given that it masks all non-causal relationships, namely all edges other than those included in the causal graph given in input). With this restriction we aim at avoiding the use of a feature's children and/or siblings that may have unstable relationships with the feature Pearl [2009] (as indeed a change in a children/siblings will not necessarily change the feature, while a change in a parent will). We plan to consider ancestors, and indirect effects to features therefrom, as future work.

To obtain a DAG from the output of Algorithm 1, we define a simple "acyclic edge creation" function that works by evaluating the strongest effect within each pair of "specular" entries in the computed adjacency matrix. In general, given a matrix $\mathbf{W} = (w_{ik})$, entries w_{ik} and w_{ki} are seen as "specular", for $i \neq k$. Formally, for any $\mathbf{W} = (w_{ik})$, we define

$$g(\mathbf{W}) = (V, E(\mathbf{W})) \quad \text{where} \quad E(\mathbf{W}) = \{(i,k) | w_{ik} > w_{ki}\} \tag{2}$$

This construction basically corresponds to taking the element-wise maximum of the lower and upper triangles of the matrix $\mathbf{W}$ across its diagonal, and eliminates "circular loops" between any two features. Note that, by construction, $g(\mathbf{W}_{\mathcal{G}}) = \mathcal{G}$, since, $\mathcal{G}$ being a DAG, at most one of w_{ik} and w_{ki} (for every $i, k \in \{1, \dots, d+1\}$) is non-zero, and this is so only if (i,k) is an edge in $\mathcal{G}$ to start with.

4.2 Working with Partial Causal Knowledge

Algorithm 1 relies upon the assumption that the input DAG is *full*, i.e. it captures, within its edges, all applicable causal knowledge: if an edge between two features is present/absent in the DAG, then the features are/are not (respectively) in a causal relationship. In this section we define a method (Algorithm 2) taking in input a graph representing relationships (between features) that *may be causal*. This graph comprises of nodes $V_p \subseteq V$ and edges $E_p \subseteq V_p \times V_p$. Intuitively, if $(i,k) \notin E_p$ then (the feature represented by) node i is definitely not in a causal relationship with (the feature represented by) node k. Thus, this graph would be *complete* [Pearl, 2009] (i.e. with exactly $V_p = V$ and $E_p = V \times V$) if no causal knowledge is available. The algorithm computes a causal DAG (as well as a network adhering to the DAG) *conforming with* the input graph $\langle V_p, E_p \rangle$, i.e. whose edges are amongst E_p. In other words, the graph represents hard constraints on the computed causal DAG, specifying edges that should not be in it.

The DAG computed by Algorithm 2 may, in addition to the input graph, accommodate *expert (causal) knowledge* from *Subject Matter Experts* (SMEs) . The possibility to receive direct (partial) human input covers more realistic scenarios, given the difficulties inherent in causal discovery, and allows humans and machines to work together: humans can provide causal information which is partial compared to the available data (i.e. not all features' interactions have a studied causal relationship in the input graph); humans can also provide feedback for the DAG learnt by our algorithm, filling gaps in the input partial DAG and rectifying the causal relations drawn from the data.

The inputs of this second algorithm are the same as Algorithm 1 with two exceptions: an input graph instead of a DAG and an additional parameter: a threshold $\tau \geq 0$ to create an initial DAG and then refine with expert knowledge. The threshold τ is used to cut out the uninfluential relationships in the data and it is applied to $\mathbf{W}$ in retrieving an intermediate DAG $\mathcal{G}_1$. To create $\mathcal{G}_1$, in the same guise as the acyclic edge creation function of Equation 2, we define another "influential and acyclic edge creation function":

$$g_\tau(\mathbf{W}) = (V, E_\tau(\mathbf{W})) \quad \text{where} \quad E_\tau(\mathbf{W}) = \{(i,k) | w_{ik} > w_{ki} \wedge w_{ik} > \tau\} \tag{3}$$

Algorithm 2 starts by creating a *base* DAG $\mathcal{G}_1$ from an adjacency matrix $\mathbf{W}$ randomly initialised or from a fitted joint network and, if non-complete, from the input graph ($\mathcal{G}_p$). When $\mathcal{G}_p$ is non-complete, we run the `DAG_inject`() function (Algorithm 1) with a (bigger) graph $\mathcal{G}_0$ conforming to $\mathcal{G}_p$. The next step is validating the causal knowledge extracted - using a function `DAG_refine`() which prompts human feedback that we refer to as *Expert Knowledge*.

Once the revised DAG $\mathcal{G}_2$ is obtained, Algorithm 1 is applied, resulting in a revised joint network and a causal DAG $\mathcal{G}_2$. Note that, by construction, $g(\mathbf{W}_{\mathcal{G}_2}) = \mathcal{G}_2$, and $\mathcal{G}_2$ conforms with $\mathcal{G}_p$ if the human feedback is consistent with $\mathcal{G}_p$; if, however, the SMEs are different from the users providing

Algorithm 2 Refine Causal DAG

Input: Training Data $\mathcal{D}$; network with M layers, h neurons in the first hidden layer, trained for t steps with final weights Θ_t; number of total training steps T; patience $T_s < T$; graph $\mathcal{G}_p = \langle V_p, E_p \rangle$; threshold τ

Function: `DAG_extract`$(\mathcal{D}, \Theta_t, T, T_s, \mathcal{G}_p, \tau)$:

$\mathbf{W} \leftarrow$ `apply`(Eq.1, Θ_t)
if $\mathcal{G}_p \neq (\varnothing, \varnothing)$ **then**
  for $i, k \in \{1, \dots d+1\}$ **do**
    if $i, k \in V_p \ \ \& \ \ (i,k) \notin E_p$ **then**
      $w_{ik} \leftarrow 0$
    end if
  end for
  $E_0 = \{(i,k) | w_{ik} > 0\}$
  $\mathcal{G}_0 = (V, E_0)$
  $\Theta_t, \mathbf{W} \leftarrow$`DAG_inject`$(\mathcal{D}, \Theta_t, T, T_s, \mathcal{G}_0)$
end if
$\mathcal{G}_1 = g_\tau(\mathbf{W})$
$\mathcal{G}_2 \leftarrow$ `DAG_refine`$(\mathcal{G}_1, \textit{Expert Knowledge})$
$\Theta_T, \mathbf{W}_{\mathcal{G}_2} \leftarrow$ `DAG_inject`$(\mathcal{D}, \Theta_t, T, T_s, \mathcal{G}_2)$
return $\mathcal{G}_2$, Θ_T

Output: $\mathcal{G}_2$, Revised weights Θ_T

$\mathcal{G}_p$ in input, then the human feedback may be inconsistent with $\mathcal{G}_p$, in which case $\mathcal{G}_2$ conforms with the components of $\mathcal{G}_p$ that the SMEs agree with. Note that once a DAG has been injected using Algorithm 1, the learnt model is guaranteed to respect it. This implies that our method "trusts" the expertise of the SMEs: we leave the study of settings where this trust is misplaced to future work (in particular, it would be intersting to study a Bayesian approach to the neural network's weights' updates, e.g. as in Mullachery et al. [2018], with the input graph as a prior to be updated through data).

To summarise the methodology and introduce the experiments, we reiterate that whilst Algorithm 1 aims at making sure that a neural network conforms to expert knowledge, Algorithm 2 has the purpose of eliciting causal knowledge from experts, so that the existing understanding of a subject can be augmented and used in causal prediction via neural networks. Note that Algorithm 2 supports two forms of human-AI collaboration: the provision of a (partial) DAG up-front and the refinement of the intermediate DAG $\mathcal{G}_1$. On the other hand, Algorithm 1 only supports the injection of a *full* DAG up-front.

5 Experiments

Here we present the results of the empirical evaluation of the proposed algorithms. The experiments are aimed at answering the following questions:

(Q1) Does causal injection by our algorithms improve predictive performance?

(Q2) How does causal injection performance change in different data (size) regimes?

(Q3) Can we reconstruct a DAG (known to be underpinning the training data) as the output of Algorithm 2?

(Q4) How well can Algorithm 2 fill the gaps of an input graph contributing only partial causal knowledge?

(Q5) How resilient are our algorithms to noise?

To answer these questions, using baselines based on CASTLE, we conduct experiments both on a regression task with synthetic data drawn from known DAGs (Section 5.2) and on classification and regression tasks on real data (Section 5.3). Before describing the design and results of the experiments, we give implementation and evaluation details (Section 5.1).

5.1 Implementation and Evaluation Metrics

We implemented our algorithms in Tensorflow extending the implementation of CASTLE.[3]

For all experiments we choose 3 hidden layers ($M = 3$) of sizes $2 * |V|, 2/3 * |V|, 2 * |V|$ respectively, with ReLU activations (experiments with smaller networks are provided in Appendix B.3). All networks are initialized and seeded identically and use the Adam optimizer with a learning rate of 0.001 for a maximum of 1000 steps. A patience (T_s) of 50 steps on the loss on the validation set is used to stop training. Results for the synthetic dataset are then reported for 10 randomly generated DAGs. For the real data experiments, given the component of hyper-parameters optimisation (the threshold τ) we have used 5-fold nested cross validation and the results reported are the average over the resulting 25 runs.

As metrics for evaluation of *predictive performance* (for questions Q1, Q2 and Q5), we use (average and Standard Deviation (Std) of) *Mean Squared Error (MSE)* for the regression tasks (with the real and synthetic data) and *Area Under the ROC Curve (AUC)* for the classification task (with the real data). As measures for evaluation of *reconstruction accuracy* (for questions Q3, Q4 and Q5), when the true DAG is known (in the case of synthetic data), we use the (distribution over the) percentage of edges that match those in the true DAG.

5.2 Experiments with Synthetic Data

Here we investigate the effectiveness of our proposed Algorithm 2 on synthetic data, when having an input graph $\mathcal{G}_p$ (supplying partial causal knowledge on the DAG $\mathcal{G}$ underpinning the Data Generating Process (DGP)), in comparison with having no a priori causal knowledge. With this set of experiments we aim at answering all the questions Q1-Q5 through the empirical evidence stemming out of a simulated environment.

Experiments Design

We apply our algorithm to synthetic data adhering to a series of randomly generated DAGs of different sizes, using the methodology of Kyono et al. [2020]. [4] The generated synthetic DAGs and data vary across three main dimensions: number of nodes in $\mathcal{G}$ ($|V| \in \{10, 20, 50\}$), number of edges ($|E| = |V| * e$,

[3] The original implementation of CASTLE we used as a starting point is https://github.com/vanderschaarlab/mlforhealthlabpub/tree/main/alg/castle.

[4] For details refer to Appendix B.1 of Kyono et al. [2020]. Note that we standardise all feature values in the generated data to mean 0 and std 1. Thus, following Reisach et al. [2021], our results can be regarded as conservative estimates of reconstruction accuracy.

where $e \in \{1, 2, 5\}$), and data size ($N = |V| * s$, where $s \in \{50, 100, 200, 300, 500\}$). In the remainder, we refer to s as *proportional sample size*. We run each scenario, involving one of the combinations of $|V|, e$ and s, 10 times and report the distribution of results as a boxplot in Figure 1, in comparison with a baseline for DAG reconstruction built from CASTLE, as follows.

Baseline DAG Reconstruction

CASTLE alone cannot be used as a baseline for DAG reconstruction, but the adjacency matrix returned by CASTLE provides a useful starting point.[5] Our baseline is thus built by: (i) using CASTLE to compute $\mathbf{W}$ according to Equation 1 and (ii) using Equation 3 to derive a DAG imposing direction and threshold, i.e. to obtain $\mathcal{G}_1 = g_\tau(\mathbf{W})$. In the remainder of the paper we call this method CASTLE+.

The differences between CASTLE+ and our Algorithms 1 and 2 are as follows. On one hand, for CASTLE+ we let CASTLE run unconstrained and then we extract a DAG through the application of Equation 3 to the $\mathbf{W}$ built applying Equation 1 to the weights Θ from CASTLE, with an appropriate choice of threshold τ. On the other hand, our method for injecting the DAG involves feeding a (possibly partial) graph into the network so that a mask is applied and only the non-masked weights are optimised.[6] In the experiments we use the value of τ that produced the lowest number of mismatches (for each of CASTLE+ and our method). Note that CASTLE+ amounts to applying Algorithm 2 with a complete graph $\mathcal{G}_p$.

Experiments

We aim at assessing Algorithm 2 against CASTLE+ according to two measures (reconstruction accuracy and prediction performance) in two scenarios (with and without noise). Deploying CASTLE+ amounts to disregarding any given a-priori causal knowledge; deploying our method instead consists of leveraging causal knowledge given up-front, while fitting networks that adhere to and discover more of it. Effectively, our experiments aim at establishing whether *injecting* causal knowledge has benefits towards the two evaluation measures, in the two scenarios.

First scenario (no noise). Following Algorithm 2, we make the initial graph $\mathcal{G}_0$ conform to the input graph $\mathcal{G}_p$ that encapsulates the pre-existent partial causal knowledge among a subset of the features involved in the model fitting. The number of edges that we inject in the experiments shown in Figure 1 is a 20% random sample of the total amount of edges in the random DAG (experiments with 10% and 50% of DAG edges injected are reported in Appendix B.4). Once the "known" edges are selected, the "specular" entries of these edges in the adjacency matrix $\mathbf{W}$ are set to 0.

The results for this scenario are given in darker colors in Figure 1, where we show the predictive performance (average MSE, represented by the bars at the bottom of the figure) and the distributions of reconstruction accuracy (the percentage of edges that matches the true DAG used to generate the data, given by the boxplots at the top of the figure). The results presented vary across one of the three dimensions mentioned earlier, namely the proportional sample size s: plots showing the changes over the other two dimensions ($|V|$ and $e = |E|/|V|$) are left to the Appendix B.1 and Appendix B.2).

Starting with the predictive performance, as visible form the bar charts at the bottom of Figure 1, the MSE for the target feature Y improves the more data is fed to the networks, but plateaus at $s = 200$. The difference in MSE between CASTLE+ and our *Injected* networks is negligible across the different proportional sample sizes. [7] As for the reconstruction accuracy, we can see from the boxplots that the overall performance again increases as s increases, though it plateaus at 300 observations per node, at an average of ~60% of right edges in the computed DAG. For $s \geq 300$ both CASTLE+ and our method achieve more than 80% reconstruction accuracy about a quarter of the times (as shown by the top lines of the boxes i.e. the 3$^{\text{rd}}$ quartile). Our method, though, reaches the plateau earlier than CASTLE+, for $s = 200$. For low data regimes ($s \leq 100$) CASTLE+ average reconstruction accuracy drops to less than 40%. The *Injected* network, instead, achieves similar performance to $s \geq 200$ with only 100 observations per node and for both $s = 50$ and 100, the amount of right edges sees more than a 1.5x average increase, considerably more than the 20% injected (as represented by the distance between the dashed lines in the boxes and the solid horizontal lines spanning across the different boxes).

Through this first set of experiments we can answer questions Q1 through Q4 positively: Algorithm 2 can improve prediction performance (Q1), with stronger gains against CASTLE+ for low data regimes (Q2); DAG reconstruction starting with no causal knowledge (CASTLE+) generally achieves fair results when enough examples per node are provided (Q3); when only lower amount of data are available though (Q4) injecting partial causal knowledge does help filling in the gaps.

Second scenario (noise). We assess the robustness of Algorithm 2 to noise, aiming at answering question Q5. To that purpose, we add to the training data a number of features amounting to 20% of the number of nodes in the DAG used to generate the data. These additional, "noisy" features are generated out of a standard normal distribution and have no links to the other features in the data . The results are again presented in Figure 1 for comparison with the first scenario. As visible from the bottom bar charts, the MSE for the target feature Y stays virtually the same regardless of proportional data size. Also on the reconstruction accuracy side (top boxplots), we can see that noise has nearly no effect on the causal discovery task. Hence we can answer question Q5 positively as well: causal injection is resilient to noise with regard to both reconstruction accuracy and predictive performance.

[5] We leverage on the reconstruction ability of CASTLE afforded by its use of NOTEARS Zheng et al. [2018]. For experiments regarding the reconstruction accuracy of NOTEARS compared to other causal discovery methodologies, please refer to Zheng et al. [2018, 2020]

[6] For an illustration of the procedure as to how we inject causal knowledge through masking, refer to Appendix A.

[7] Note that here we are actually using CASTLE directly, because we do not need to apply Equation 3 to measure MSE. See Kyono et al. [2020] for comparative results of CASTLE's predictive performance against all SOTA regularization techniques.

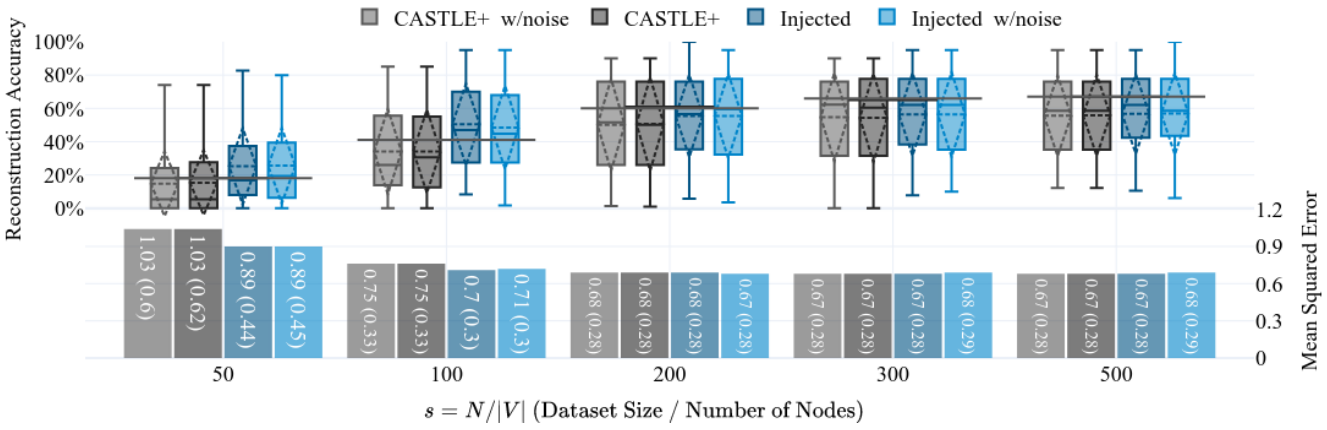

Figure 1: Reconstruction Accuracy and MSE when changing $s = N/|V| \in \{50, 100, 200, 300, 500\}$, the sample size N proportional to the number of nodes $|V| \in \{10, 20, 50\}$ in the causal DAG $\mathcal{G}$. Darker (grey or blue) colors refer to the no-noise scenario, whereas lighter (grey or blue) colors refer to the scenario with noise (w/noise). The values are an average over 10 runs for each combination of $|V|, s$ and $e = |E|/|V| \in \{1, 2, 5\}$. The boxplots (left y axis) show Min/Max/Median (solid lines) and Mean/Std (dashed lines) of the reconstruction accuracy. The bottom bars (right y axis) show the MSE (std). The solid horizontal lines spanning across each of the pairs (CASTLE+ vs Injected) of boxplots are the re-based value of the CASTLE+ mean to account for the advantage that our Injection methodology knows 20% of the edges. If the mean of *Injected* is above/below the level of the horizontal lines, the average increase in reconstruction accuracy is more/less than proportional to the amount injected.

5.3 Experiments with Real Data

We carried out the second set of experiments on real financial data from four different publicly available datasets (see details in Appendix C): two classification and two regression tasks. For the classifications, we use the FICO HELOC data FICO [2017] for *credit risk* assessment (answering the question of whether an applicant is to be accepted for a loan) and the Adult Income dataset Kohavi et al. [1996], useful for affordability checks in the lending business (predicting whether the income of a person is greater than USD50K). The two regression tasks are instead about predicting median house prices: we used the well known Boston Harrison and Rubinfeld [1978] and California Pace and Barry [1997] Housing datasets. Specifically, we report analysis for three experiments using Algorithm 2 (i) with no prior causal knowledge and reconstructing a *full* DAG to then inject it into our networks; (ii) with partial causal knowledge (for the Adult dataset) expressing basic causal (or common sense) assumptions, and (iii) to refine the DAG extracted in (i) with the assumptions adopted in (ii). In the absence of a true DAG representing the causal relationships for the problems underlying these data, the questions we are going to answer here are only regarding predictive performance i.e. Q1 and Q2. We leave experiments on real-world DAGs as future work.

First Experiment (Full DAG Discovery and Injection) We construct a potential DAG $\mathcal{G}_1$ (using Algorithm 2 with a complete input graph, i.e. no a priori causal knowledge) and then inject it to measure the resulting predictive performance with and without injection. Within the $g_\tau(\mathbf{W})$ function in Algorithm 2, we tried many different thresholds τ and chose the "best" DAG for injection through the evaluation of the change in predictive performance (for details of this evaluation see Figure 7 in Appendix C.1): for each dataset, we select the DAG with lowest MSE/highest AUC and, as tie breaker, the lowest number of edges in the computed DAG. An example of extracted DAG, for the Adult dataset, is shown in Figure 3. Within Algorithm 2, we fed the chosen DAGs as $\mathcal{G}_2$ into `DAG_inject()` (Algorithm 1) to make the *Injected* network compliant with the "causal view of the data" expressed by the computed DAG. We aimed at checking whether fixing a (plausible though not humanly validated) DAG can lead to better predictive performance and whether its level depends on data size (questions Q1-Q2).

Results As seen in Table 1, the predictive performance of the *Injected* networks on real data can be significantly better than CASTLE. Indeed, AUC for the Adult dataset is consistently above CASTLE while using only ~20% of the relationships that the "unconstrained" network uses (similarly for the Boston data, though we only have a maximum of 500 observations, amounting to $s = N/|V| = 35$). For the California dataset, the MSE is better for all sample sizes but the biggest, where CASTLE achieves a better performance: here the reduction of computed DAG's edges is about 40% of the "unconstrained" network.[8] The worst results in terms of predictive performance are observed in the HELOC dataset . Here, the AUC for the *Injected* network is predominantly lower than CASTLE, though at most by 0.1 and with a much sparser network (the amount of first layer's weights used for prediction is only 15% of the "unconstrained" CASTLE network). We note that, by *minimality* Pearl [2009] or *parsimony* Vandekerckhove et al. [2015], when the performance stays equal, a modeller should prefer the sparser, more parsimonious model.[9]

[8] This reduction matches the reduction in networks' weights at the input layer.

[9] According to Pearl [2009], "performance" here is about the equivalence of the probability distributions generated by the different sets of edges in the computed latent structures.

Table 1: Experiments with real data in the financial/economics sector. We report MSE (AUC) for regression (classification) across different sample sizes of the training data (best results in bold). We also detail, for each dataset, the number of features/nodes $|V|$ and the number of edges $|E|$ in the injected DAG (for our method) and in the (graph drawn from the) underlying adjacency matrix (for CASTLE). NA indicates a data size (N) bigger than the full dataset. CASTLE and *Injected* columns refer to Section 5.3, for *Partial* and *Refined* columns see Sections 5.3 and 5.3, respectively.

	REGRESSION (Metric: MSE)				**CLASSIFICATION (Metric: AUC)**					
	California ($\|V\| = 8$)		**Boston** ($\|V\| = 14$)		**HELOC** ($\|V\| = 23$)		**Adult** ($\|V\| = 14$)			
Data	**CASTLE**	***Injected***	**CASTLE**	***Injected***	**CASTLE**	***Injected***	**CASTLE**	***Injected***	***Partial***	***Refined***
(N)	$\|E\| = 72$	$\|E\| = 31$	$\|E\| = 182$	$\|E\| = 48$	$\|E\| = 552$	$\|E\| = 85$	$\|E\| = 210$	$\|E\| = 46$	$\|E\| = 116$	$\|E\| = 30$
100	7.05 (12.81)	**2.94 (2.63)**	112.04 (91.06)	**86.17 (13.75)**	**0.75 (0.02)**	0.74 (0.04)	0.67 (0.03)	**0.69 (0.04)**	0.66 (0.02)	**0.69 (0.04)**
500	2.33 (1.39)	**2.25 (1.07)**	21.95 (6.84)	**20.45 (5.12)**	**0.79 (0.01)**	0.78 (0.01)	0.72 (0.04)	**0.74 (0.02)**	0.71 (0.02)	**0.74 (0.02)**
1000	2.96 (4.12)	**1.68 (1.14)**	NA	NA	0.78 (0.01)	0.78 (0.01)	0.75 (0.03)	**0.76 (0.03)**	0.74 (0.03)	**0.76 (0.02)**
2000	3.86 (3.68)	**1.71 (0.57)**	NA	NA	**0.79 (0.01)**	0.78 (0.01)	0.74 (0.03)	**0.77 (0.01)**	**0.76 (0.03)**	**0.77 (0.02)**
5000	4.91 (7.41)	**1.51 (0.62)**	NA	NA	0.79 (0.01)	0.79 (0.01)	0.75 (0.03)	**0.79 (0.03)**	**0.76 (0.02)**	**0.79 (0.03)**
10000	1.74 (1.70)	**1.16 (0.31)**	NA	NA	**0.80 (0.01)**	0.79 (0.01)	0.75 (0.02)	**0.85 (0.01)**	**0.76 (0.02)**	**0.85 (0.01)**
20000	**0.66 (0.08)**	1.02 (0.35)	NA	NA	NA	NA	0.76 (0.02)	**0.86 (0.01)**	**0.77 (0.02)**	**0.86 (0.01)**

Discussion Simulating the use of Algorithm 2 on real data demonstrated its capability to remove an average of ~75% of the edges in a potential DAG, with respect to CASTLE, while generally improving predictive performance (quite significantly) or, in the worst case, losing at most 1% (but with much more parsimonious models).

Note that our strategy for choosing the DAGs to inject is purely mechanic for this set of experiments. As expected, the smaller the DAG injected, the lower the amount of relations that the network can leverage on for prediction, hence the lower the performance thereof (see Figure 7 in Appendix C.1). The adopted strategy is meant to assess the results in predictive performance of the *Injected* networks without involving a qualitative assessment of the validity of the causal assumptions, that SMEs should carry out. We envisage this strategy as a useful starting point in the absence of a priori causal knowledge. However, in real life applications, we intend the use of Algorithm 2 by (a panel of) expert(s) iteratively assessing intermediate outputs to refine their views in light of previous experiments and, most importantly, their experience and knowledge of the problem at hand.

In the remainder of this section we introduce two experiments providing examples of how Algorithm 2 can work in a human-AI collaboration setting. We run these experiments on the Adult dataset, as it contains only 14 input features, some of which (notably *race, sex, age* and *native-county*) lending themselves to the construction of (common sense) causal assumption by lay users.

Second Experiment (Inject Partial Knowledge)

In this experiment, instead of the "automated" procedure for producing DAGs adopted in the experiment of the previous section, we go back to first principles and build a very simple yet intuitive input graph $\mathcal{G}_p$ for the Adult dataset. Through $\mathcal{G}_p$ we effectively constrain the network to respect the following assumptions (reflected in the adjacency matrix depicted in Figure 2):

- *race, sex, age, native-county* cannot be caused by any feature (columns 2 to 5 of the adjacency matrix in Figure 2 are blanked i.e. these features cannot have incoming edges);
- *occupation* and *hours-per-week* cannot cause *fnlwgt (demographics index), education, education-num, relationship* and *marital-status* (the respective cells in Figure 2 are blanked);
- the target ($salary > USD50K$) cannot cause any feature and *capital-gain, capital-loss* none apart from the target (rows 1, 13 and 14 in Figure 2 are blanked).

Note that some of these assumptions could easily be confuted, e.g. by arguing that the target *can* cause features, such as *capital-gain* and *loss*; we adopt these assumptions only to illustrate the effects on the adjacency matrix and to simulate a scenario whereby the modeller is testing whether the algorithm finds relationships in the data that help the prediction task.[10]

Given the absence of ground truth for the DAG underlying these data, our evaluation revolves around the predictive performance of the *Injected* networks across increasing sample sizes (N). We report predictive performance in Table 1, *Par-*

[10] As in Pearl [2009], we believe that the opportunity to extract and enforce such assumptions, or simply talk about them, has the potential to make models more robust and representative of human thinking and understanding.

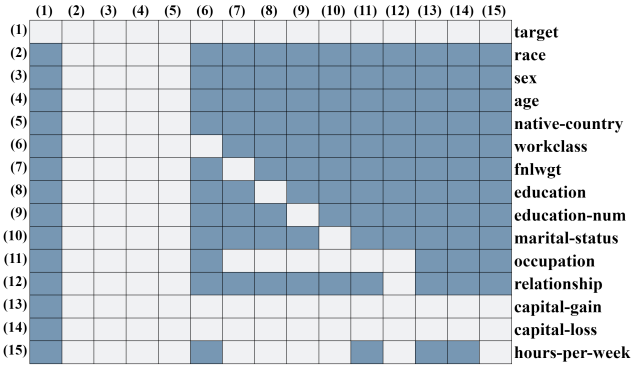

Figure 2: Input graph $\mathcal{G}_p$, as partial causal knowledge for the Adult dataset, in the form of an adjacency matrix $\mathbf{W}$. Blue represents edges; missing edges in white (hard constraints).

tial column: the "causal constraints" result in performances at most 1% worse than our baseline with smaller samples ($N \leq 1000$), and comparable performance for bigger samples, but with a computed DAG that has about a half the edges of the "unconstrained" one (116 vs 210). On the whole, we obtain a sparser network, adherent to common-sensical causal knowledge following our assumptions, whose recommendations are therefore arguably more understandable and trustworthy, and whose performance is comparable to an "unconstrained" one.

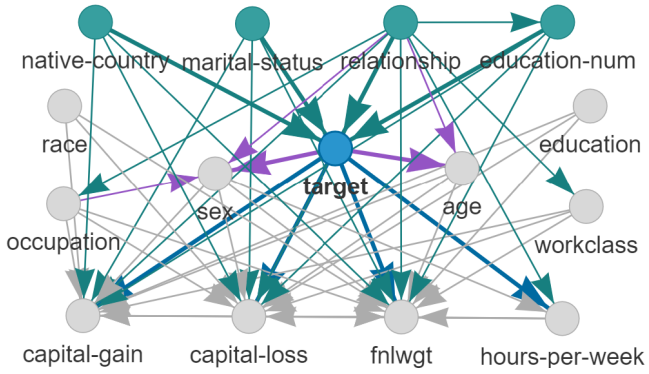

Figure 3: Example of computed DAG for Adult dataset (see Section 5.3). Cyan nodes at the top are computed causes for the target ("Income>50K"), edges coming out of the target are in blue while in purple are the edges into nodes that cannot be caused (as per basic assumptions in Section 5.3).

Third Experiment (Refine Computed DAG)
The final experiment continues that of Section 5.3 on the Adult dataset, and amounts to an exemplification of the use of the `DAG_refine()` function in Algorithm 2. This function takes in input a DAG $\mathcal{G}_1$ and what we call *Expert Knowledge*. As $\mathcal{G}_1$ we use the DAG depicted in Figure 3: this is obtained through the iterative procedure involving the optimisation of the threshold τ, within the experiment presented in Section 5.3 (see Appendix C.1 for details). In this DAG, the target feature is deemed to be causing a few others (blue and thick purple edges in Figure 3), with sex and age among them (purple edges).

This is counter-intuitive from a common sense (let alone causal) perspective. In this experiment we explore the effect of injecting a revised DAG $\mathcal{G}_2$ without those edges. The results, in Table 1, *Refined* column, are again very compelling: the network injected with the refined DAG is not only more intuitive and adhering to common sense, but presents the same predictive performance as the network using non-sensical relationships (and substantially better performance than the "unconstrained" one). Ultimately, our network is 7 times smaller (than CASTLE, in the input layer), adheres to common sense, and yet it is significantly more performing than an "unconstrained" network.

6 Conclusion

We have introduced two algorithms to perform causal discovery and injection for feed-forward neural networks. We leverage on the model structure of [Kyono et al., 2020] and improve its causal representation guarantees by making the networks adhere to an input graph. This can be given in full or partially, or we can leverage the causal graph discovery within CASTLE itself to initialise it. Once given this input graph, our method provides a framework for humans to refine it and inject it into the final model. The proposed methods represent a principled way of fitting neural networks with limited knowledge about the causal links in the data, without hindering predictive performance (and possibly improving it) but paving the way towards users' understanding of the relationships that the network is leveraging on to arrive at its predictions. Furthermore, we demonstrate, through empirical results on synthetic data, that causal injection generally improves causal discovery, above all in low data regimes as well as being quite resilient to noisy data. Finally, we apply our algorithms to real financial datasets demonstrating how they can yield very parsimonious networks (hence more interpretable and easier to debug) while either significantly improving predictive performance or losing very little thereof.

We see interesting lines of future work to develop the presented methodology further. It would be interesting to explore the functional relationships that the networks learn for each of the edges of the DAG (i.e. full causal models, rather than simply graphs); this would require accommodating the estimation of causal effects (e.g. by integrating our masking scheme with the one by Germain et al. [2015], Xia et al. [2021]). It would also be useful to introduce Bayesian learning weight updates (e.g. as in Mullachery et al. [2018]) to improve our method's human-AI collaboration capabilities by allowing for mistakes in the injected DAG. We also plan to explore the human-in-the-loop debugging capabilities of our method, especially for high-stakes decision models, as in the financial or healthcare settings. In particular, we wish to see our algorithms, and the human-AI collaboration framework they support, used and improved upon by both the academic and industrial communities, possibly leading to Random Controlled Trials (RCTs) that help inform some of the missing knowledge, to then be complemented by our discovery algorithms. Finally, it would be interesting to study the use of the (fully or partially) injected DAG into a neural network as a vehicle for explaining its outputs.

Acknowledgments This research was partially funded by UKRI [grant number EP/S0233356/1], in the CDT in Safe and Trusted AI, by J.P. Morgan and by the Royal Academy of Engineering under the Research Chairs and Senior Research Fellowships scheme and by the European Research Council (ERC) under the European Union's Horizon 2020 research and innovation programme (grant agreement No. 101020934, ADIX). Any views or opinions expressed herein are solely those of the authors.

References

D. Alvarez-Melis and T. S. Jaakkola. A causal framework for explaining the predictions of black-box sequence-to-sequence models. In *Proc. EMNLP*, 2017.

T. Aste and T. Di Matteo. Sparse causality network retrieval from short time series. *Complexity*, 2017, 2017.

Y. Bengio, T. Deleu, N. Rahaman, R. Ke, S. Lachapelle, O. Bilaniuk, A. Goyal, and C. Pal. A meta-transfer objective for learning to disentangle causal mechanisms. In *Proc. ICLR*, 2019.

A. Chattopadhyay, P. Manupriya, A. Sarkar, and V. N. Balasubramanian. Neural network attributions: A causal perspective. In *Proc. ICML*, 2019.

FICO. Fico xml challenge found at community.fico.com/s/xml, 2017. URL https://community.fico.com/s/explainable-machine-learning-challenge.

M. Germain, K. Gregor, I. Murray, and H. Larochelle. Made: Masked autoencoder for distribution estimation. In *Proc. ICML*, 2015.

C. Glymour, K. Zhang, and P. Spirtes. Review of causal discovery methods based on graphical models. *Frontiers in genetics*, 10:524, 2019.

I. Goodfellow, Y. Bengio, and A. Courville. *Deep Learning*. MIT Press, 2016. http://www.deeplearningbook.org.

I. J. Goodfellow, J. Shlens, and C. Szegedy. Explaining and harnessing adversarial examples. *arXiv preprint arXiv:1412.6572*, 2014.

O. Goudet, D. Kalainathan, P. Caillou, I. Guyon, D. Lopez-Paz, and M. Sebag. Causal generative neural networks. *arXiv preprint arXiv:1711.08936*, 2017.

R. Guo, L. Cheng, J. Li, P. R. Hahn, and H. Liu. A survey of learning causality with data: Problems and methods. *ACM Computing Surveys (CSUR)*, 53(4):1–37, 2020.

D. Harrison and D. Rubinfeld. Hedonic housing prices and the demand for clean air. *Journal of Environmental Economics and Management*, 5:81–102, 03 1978.

D. Heckerman. A bayesian approach to learning causal networks. *arXiv preprint arXiv:1302.4958*, 2013.

D. Heckerman, D. Geiger, and D. M. Chickering. Learning bayesian networks: The combination of knowledge and statistical data. *Machine learning*, 20(3):197–243, 1995.

R. Kohavi et al. Scaling up the accuracy of naive-bayes classifiers: A decision-tree hybrid. In *Proc. KDD*, 1996.

T. Kyono, Y. Zhang, and M. van der Schaar. Castle: Regularization via auxiliary causal graph discovery. In *Proc. NeurIPS*, 2020.

S. Lachapelle, P. Brouillard, T. Deleu, and S. Lacoste-Julien. Gradient-based neural dag learning. In *Proc. (ICLR)*, 2020.

Z. Li, X. Ding, K. Liao, T. Liu, and B. Qin. Causalbert: Injecting causal knowledge into pre-trained models with minimal supervision. *arXiv preprint arXiv:2107.09852*, 2021.

V. Mullachery, A. Khera, and A. Husain. Bayesian neural networks. *arXiv preprint arXiv:1801.07710*, 2018.

M. Nauta, D. Bucur, and C. Seifert. Causal discovery with attention-based convolutional neural networks. *Machine Learning and Knowledge Extraction*, 1(1):312–340, 2019.

R. K. Pace and R. Barry. Sparse spatial autoregressions. *Statistics & Probability Letters*, 33(3):291–297, 1997.

N. Pawlowski, D. Coelho de Castro, and B. Glocker. Deep structural causal models for tractable counterfactual inference. In *Proc. NeurIPS*, 2020.

J. Pearl. *Causality*. Cambridge University Press, 2 edition, 2009.

J. Pearl and T. Verma. A theory of inferred causation. In *KR, Second International Conference conference on the Principles of Knowledge Representation and Reasoning, Cambridge, Massachusetts, April 1991*, 1991.

A. Reisach, C. Seiler, and S. Weichwald. Beware of the simulated dag! causal discovery benchmarks may be easy to game. In *Proc. NeurIPS*, 2021.

C. Rudin. Stop explaining black box machine learning models for high stakes decisions and use interpretable models instead. *Nature Machine Intelligence*, 1(5):206–215, 2019.

B. Schölkopf. Causality for machine learning. *arXiv preprint arXiv:1911.10500*, 2019.

P. Schwab and W. Karlen. Cxplain: Causal explanations for model interpretation under uncertainty. In *Proc. NeurIPS*, 2019.

P. Spirtes, C. Glymour, and R. Scheines. *Regression, Causation and Prediction*, pages 238–258. Springer New York, New York, NY, 1993. ISBN 978-1-4612-2748-9.

C. Szegedy, W. Zaremba, I. Sutskever, J. Bruna, D. Erhan, I. Goodfellow, and R. Fergus. Intriguing properties of neural networks. *arXiv preprint arXiv:1312.6199*, 2013.

J. Vandekerckhove, D. Matzke, and E.-J. Wagenmakers. 14 model comparison and the principle of parsimony. *The Oxford Handbook of COMPUTATIONAL and*, page 300, 2015.

M. J. Vowels, N. C. Camgoz, and R. Bowden. D'ya like dags? a survey on structure learning and causal discovery. *arXiv preprint arXiv:2103.02582*, 2021.

K. Xia, K.-Z. Lee, Y. Bengio, and E. Bareinboim. The causal-neural connection: Expressiveness, learnability, and inference. In *Proc. NeurIPS*, 2021.

C. Zhang, K. Zhang, and Y. Li. A causal view on robustness of neural networks. In *Proc. NeurIPS*, 2020.

X. Zheng, B. Aragam, P. K. Ravikumar, and E. P. Xing. Dags with no tears: Continuous optimization for structure learning. In *Proc. NeurIPS*, 2018.

X. Zheng, C. Dan, B. Aragam, P. Ravikumar, and E. Xing. Learning sparse nonparametric dags. In *Proc. AISTATS*, 26–28 Aug 2020.

S. Zhu, I. Ng, and Z. Chen. Causal discovery with reinforcement learning. In *Proc. ICLR*, 2020.

Appendices

A Masked Joint Neural Network

We provide in Figure 4 a schematic of the neural structure in Kyono et al. [2020] (see Section 3) that our algorithms build

upon (see Section 4). The structure of the *joint* neural network amounts to: an input layer of size $(d+1) \times d$ because each of the $d+1$ sub-networks have at least one input neuron masked (greyed out node, corresponding to the output node). The hidden layers are shared and encode information from all sub-networks. The output layer has dimension $d+1$. We highlight in black the connections of sub-network 1 (predicting Y with $X_1, \ldots, X_d$)) as an example. We extend the masking scheme from Kyono et al. [2020] by making it encode the answers to causal questions like the one in Figure 4: *does the edge (and therefore the weight) from X_1 to Y belong to our approved causal structure $\mathcal{G}$?* If so then masking is not applied, otherwise we put that weight to 0.

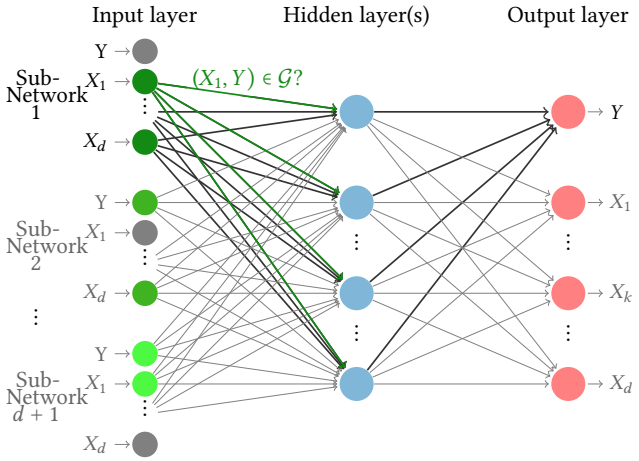

Figure 4: Joint Neural Network Structure. Darker arrows refer to the highlighted Sub-Network 1, predicting Y (Output layer), while having Y masked (grayed out in Input layer). In green we show the weights (arrows) we consider masking when injecting the causal structure from the input graph.

B Parameters' Study for the Experiments with Synthetic Data

The results reported in Section 5.2 show variation only wrt one of the dimensions considered when generating the random DAGs and data, namely, proportional sample size ($s = N/|V|$). Here, we report additional results for the other two dimensions: number of nodes $|V|$ (Section B.1), and proportion of edges over nodes $e = |E|/|V|$ (Section B.2). Additionally, we provide comparisons for other two parameters: network size (Section B.3) and the percentage of edges injected (Section B.4). The results of this section corroborate the ones presented in Section 5.2.

B.1 Number of Nodes in the DAG

MSE and reconstruction accuracy results when changing $|V|$ are shown in Figure 5 ($M = 3$ correspond to the main scenario, as in Figure 1). We can observe that the performance varies significantly for increasing DAG sizes. For $|V| = 10$, both CASTLE+ and our method show better reconstruction accuracy than the average across s (see Section 5.2); for $|V| > 10$, though, we observe a significant drop in overall performance

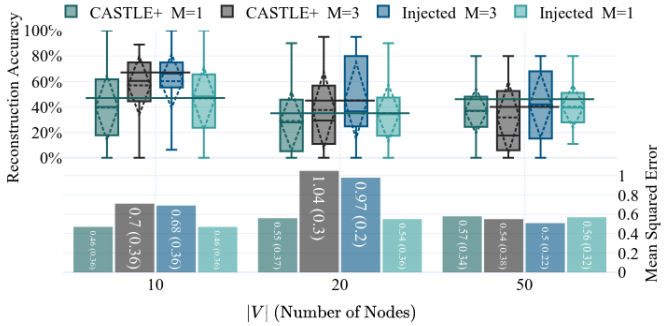

Figure 5: Reconstruction Accuracy and MSE when changing the number of nodes in the DAG underpinning the data (see Section B.1), with different numbers of layers (M=3 as in the paper, see Figure 1) (see Section B.3).

for CASTLE+, whereas our method suffers less from the increased size of the problem.

B.2 Number of Edges in the DAG

The effect of changing the proportion of edges per node ($e = |E|/|V|$) is presented in Figure 6 (CASTLE+ vs Injected 20% which is the scenario shown in Figure 1 in the main text). Results show that the sparser the DAG (the smaller e) the better the performance of the algorithm, achieving reconstruction accuracy averaging at around 75% for $e = 1$. For $e = 2$ the average drops to the average level across all proportional sample sizes s, while increasing e further, to 5, results in averages dropping to less then 40%, comparable to the effect of having only 50 observations per node ($s = 50$, Figure 1). Overall, the denser the DAG, the worse the performance of both CASTLE+ and our algorithms.

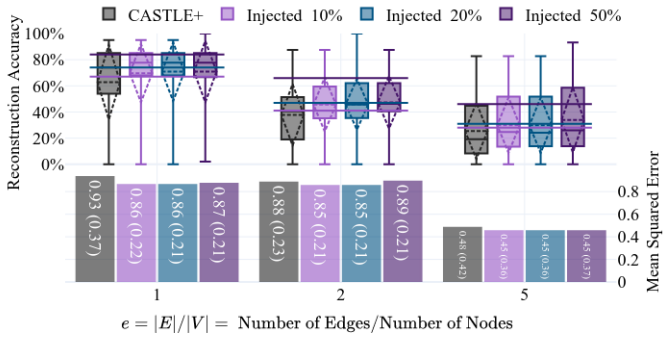

Figure 6: Reconstruction Accuracy and MSE when changing the proportion of edges over nodes (see Section B.2). The amount of known edges injected is 10%, 20% (as in the paper, see Figure 1) and 50% (see Section B.4).

B.3 Network Size

In Figure 5, jointly with the nodes' analysis, we show a comparison of 3-layers networks (used for the experiments in Section 5.2) with smaller networks of one single hidden layer and an amount of neurons of 3.2 times the number of input features (i.e. $M = 1, h = (d+1) * 3.2$). As visible from the bottom bar charts, and quite surprisingly, the MSE for the target variable Y is generally smaller with smaller networks, while increasing the network size positively affects causal discovery.

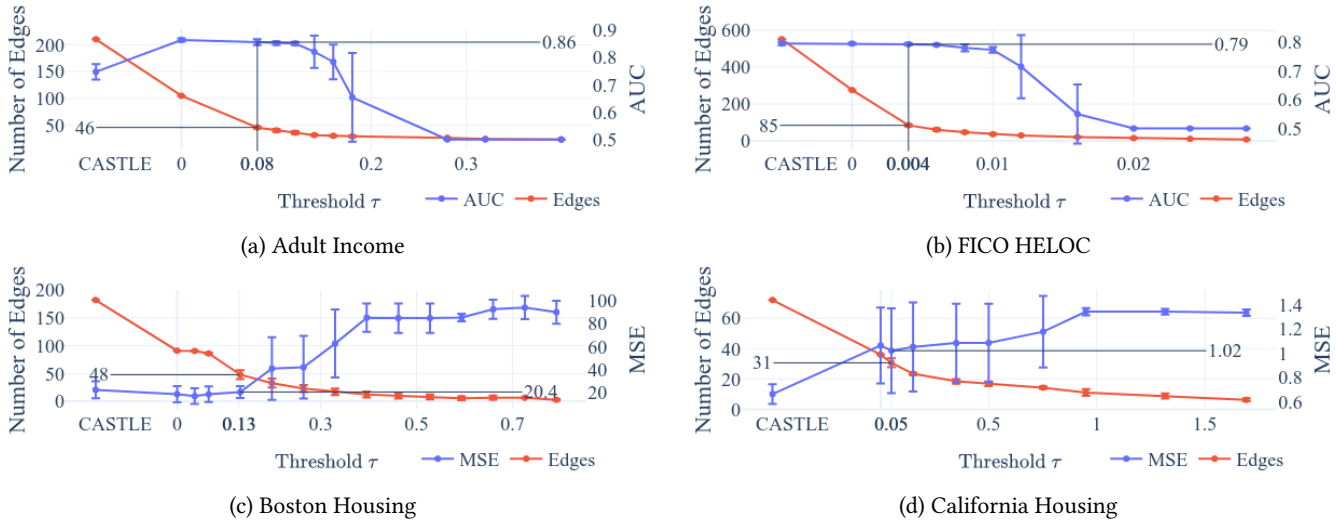

(a) Adult Income

(b) FICO HELOC

(c) Boston Housing

(d) California Housing

Figure 7: Threshold τ optimisation forexperiment in Section 5.3. Here $\tau < 0$ corresponds to the application of "unconstrained" CASTLE Kyono et al. [2020]. Chosen thresholds are in bold on the x-axis. The number of edges and the predictive performance of the network injected with the DAG derived with the chosen τ are reported on the y-axes.

B.4 Percentage of Known Edges

Finally, in Figure 6 we vary the proportion of edges injected (10%, 20% as in the main text, and 50%). As visible, injecting 50% of noise never pays off proportionally, i.e. the average reconstruction accuracy, although higher than CASTLE+, generates less of an increase than "rebased" CASTLE (solid horizontal lines). On the other hand, the reconstruction accuracy when injecting 10% of the DAGs is always more than proportional to the injected amount. Most of the gains are recorded for denser DAGs ($e \in \{2, 5\}$) when reconstruction is generally more difficult (as shown by the decreasing overall trend).

C Further Details for Experiments with Real Data

Here we provide additional details for the experiments in Section 5.3: about the datasets herein and, in Section C.1, around the optimisation of the threshold τ (part of the experiment in Section 5.3).

The details for the data used are in Table 2. For the regression tasks we downloaded the data (Boston Housing [Harrison and Rubinfeld, 1978]and California Housing [Pace and Barry, 1997]) from scikit-learn[11] and used it as-is. We used instead pre-processed data for the classification tasks (Home Equity Line Of Credit[12] [FICO, 2017] and Adult Income[13] [Kohavi et al., 1996]). For Adult, we sampled 20000 observations and we balanced the proportion of positive and negative examples in target feature to 50-50 (from 25-75).

[11]https://scikit-learn.org/stable/datasets/toy_dataset.html

[12]Data and pre-processing mapping (keys.csv) is downloadable from our repo at https://anonymous.4open.science/r/causal-injection/data/fico;

[13]Data and pre-processing mapping are from Penn Machine Learning Datasets repository at https://github.com/EpistasisLab/pmlb/blob/master/datasets/adult/

Table 2: Real-world dataset details. Type is Regression (R) for real-valued target or Classification (C) for binary target.

Dataset	Sample Size	Features	Type
Boston Housing (BH)	506	14	R
California Housing (CH)	16512	8	R
Home Equity Line Of Credit (HELOC)	7844	23	C
Adult Income (IN)	48842	14	C

C.1 Threshold Optimisations

Here we provide details on the optimisation of the threshold τ to chose a DAG without having to make qualitative causal judgments. The results for all datasets are in Figure 7. The optimisation runs through several thresholds and compares the number of edges (red) and the appropriate predictive performance metric (blue) when increasing the threshold τ (along the x axis) so that more and more edges are masked. All the red lines expectedly decrease monotonically, while the MSE/AUCs are the trends of interest.

As visible in Figure 7a for the Adult dataset, $\tau = 0.08$ keeps the best AUC, while reducing the number of edges by more than 50% compared to $\tau = 0$. Increasing τ produces small gains in parsimony (lower $|E|$) but starts to reduce performance. The same applies to the FICO HELOC data in Figure 7b, where we select $\tau = 0.004$, before the AUC started to decrease. For both a valid alternative could have been $\tau = 0.1$ and 0.01, respectively, but we preferred a lesser worsening of performance for small gains in parsimony. For the Boston dataset in Figure 7c, we select $\tau = 0.13$ as the MSE thereafter increases significantly. Finally, California (Figure 7d) shows a different scenario: injecting always hurts predictive performance. We chose $\tau = 0.05$ which has the lowest MSE. As visible in Table 1 though, the lower MSE is not observed for smaller sample sizes.